CrystEngComm

PAPER

View Article Online
View Journal | View Issue

Cite this: *CrystEngComm*, 2014, **16**, 9842

The effect of NH_4^+ on shape modulation of $La_{1-x}Sr_xMnO_3$ crystals in a hydrothermal environment

Keke Huang,[a] Wenchun Feng,[b] Long Yuan,[a] Jiaxin Zhang,[a] Xuefeng Chu,[ac] Changmin Hou,[a] Xiaofeng Wu[a] and Shouhua Feng*[a]

Received 30th June 2014,
Accepted 20th August 2014

DOI: 10.1039/c4ce01332h

www.rsc.org/crystengcomm

Perovskite oxide ($La_{1-x}Sr_xMnO_3$) crystal facet control is rarely reported due to difficulties in modulation, even though it is highly important in surface-dependent catalytic and electrochemical applications. In this paper, we present the shape diversity of $La_{1-x}Sr_xMnO_3$ crystals evolved from a hydrothermal environment when urea is used as an effective facet modulator. By changing the La/Sr ratio from 1 to 3, the structure changes from pseudo-cubic to $P2_1/a$ monoclinic, induced by the evolution processes of different facets during crystallization. Our proposed hypothesis is that the NH_4^+ interaction with octahedral MnO_6 may be beneficial in enhancing the activity of $La_{1-x}Sr_xMnO_3$ for applications, and moves toward strategies for the development of highly active perovskite oxides.

1. Introduction

Naturally grown crystals from liquid environments often form shapes with well-defined facets, edges and vertices,[1–5] which demonstrates that shape control of crystals is crucial for the modulation of facet growing speed at the atomic scale.[1] Much effort for modulating crystal facets has been made due to their relevance in catalytic,[2] sensor,[3] antibacterial activity,[4] and cancer treatment[5] applications. Crystal facet evolution is determined by the crystal's growth environment. Usually surfactants and ionic capping agents are used as an effective method for modulating the corresponding plane attachment. Most previous reports concentrate on noble metal nanocrystals (*e.g.* Pd,[6] Pt,[7] Au[8]) as well as simple binary oxides (*e.g.* Cu_2O,[4,9] TiO_2,[10] Co_3O_4 [11]) and fluorides (*e.g.* YF_3 [12]) because of their relatively simpler arrangements of atoms in crystal lattices. In our previous work, crystal facet control of $LaFeO_3$, $LaCrO_3$ and $La_{0.75}Sr_{0.25}MnO_3$ were achieved,[13] however, up to now, few articles have been reported on complex system oxides, such as perovskite (involving BO_6 octahedral vertex connections with A-site cations inserted to retain the stable structure), which may result from more complex interatomic interactions. Fundamental understanding of crystal facet modulation mechanisms is still lacking at the atomic/molecular level, therefore, in-depth investigation in these systems is much needed.

Shape control of crystal growth has been reported for various types of oxide materials by modulating reactive conditions in the liquid phase.[14] An effective route to crystal facet modulation is introducing various anionic/cationic surfactant or polymer molecules in crystal growth, such as sodium cetyltrimethylammonium bromide (CTAB),[15] sodium dodecylbenzene sulfonate (SDBS)[16] and polyvinyl pyrrolidone (PVP).[3,8] Polyethylene glycol (PEG) was also introduced to modulate the shapes of $BiFeO_3$ [17]and $BaTiO_3$.[18] Self-propagating high-temperature synthesis[19] and the molten salt method were used to obtain various shapes of $SrTiO_3$,[20] which shows facet-dependent water-splitting catalytic activity. The shaping effect of NH_4^+ has been recognized in many compounds prepared in liquid phase processes, such as WO_3,[21] MoO_3 [22] and TiO_2.[23] However, the crystal facet-directing effect of NH_4^+ has not been recognized in complex perovskite oxides. Traditionally, KOH (as a mineralizer) has often been used to provide an OH^- environment in the hydrothermal crystallization process of ABO_3 perovskite,[24] which makes the final crystal a cubic shape enclosed with {100} facets of A–O (La–O or Sr–O) layers.[25] The A–O layer on the surface is cationic with positive charges due to the coordinatively unsaturated La^{3+} and Sr^{2+}, which draw anions to attach and bond to this layer, thus making this surface more stable.[26] The BO_6 octahedron, however, is anionic with negative charges, balanced by A^{n+} cations inside of the crystal and positive K^+ cations (which have highly symmetric, spherical electrical fields) at the interface of crystal and liquid.

[a] *State Key Laboratory of Inorganic Synthesis and Preparative Chemistry, College of Chemistry, Jilin University, Changchun 130012, PR China. E-mail: shfeng@mail.jlu.edu.cn; Fax: +86 431 85168624; Tel: +86 431 85168661*
[b] *Department of Chemistry and Chemical Biology, Rutgers University, Piscataway, New Jersey 08854, USA*
[c] *Department of Basic Science, Jilin Jianzhu University, Changchun 130118, PR China*

By introducing NH_4^+ (tetrahedral in shape, non-spherical electrical field) to this system, the attraction between NH_4^+ and the BO_6 octahedra blocks further crystal growth on the neighbouring sites (Scheme 1), which slows down relative crystal facet growing speed and keeps these facets in their final shape.

$La_{1-x}Sr_xMnO_3$ (LSMO) has a stable structure and is a promising alternative for noble metal catalysts. In particular, it is an effective catalyst in CH_4 and CO combustion[27] and NO_x reduction,[28] and the orientation of the $La_{1-x}Sr_xMnO_3$ {100} film is highly influential on its oxygen reduction reaction activity.[29] In our previous report, $La_{0.7}Sr_{0.3}MnO_3$ magnetic hollow micro-spheres with complex units were formed in a hydrothermal environment by self-construction.[30] Morphology-dependent catalytic activity towards CO oxidation and CH_4 combustion were confirmed in $La_{0.75}Sr_{0.25}MnO_3$ fibres and nanoparticles.[31] Recently, we recognized that urea is an effective plane-directing agent in controlling the facets of perovskite-structured single crystals.[13] In this paper, studies of urea-affected LSMO shape evolution were carried out to yield a more fundamental understanding of the versatile shapes possible in complex environments. The method of modulating crystal growth and preparation using ions with non-spherical electrical fields opens up strategies for the development of other highly active perovskite oxides.

2. Experimental

The chemicals $La(NO_3)_3{\cdot}6H_2O$ (99.9%), $Sr(NO_3)_2$ (99.9%), $KMnO_4$, $MnCl_2{\cdot}4H_2O$, $CO(NH_2)_2$ (99.99%), and analytical reagent grade KOH were purchased from Sinopharm Chemical Reagent Co. Ltd. and were used without further purification. Solutions of 0.4 M $La(NO_3)_3$, $Sr(NO_3)_2$, 0.36 M $KMnO_4$ and 0.56 M $MnCl_2$ were prepared in deionized water in advance.

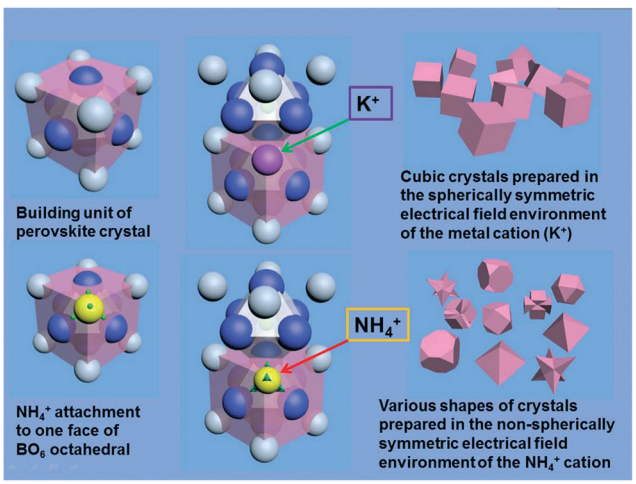

Scheme 1 Evolution of perovskite crystal shapes in hydrothermal environments: according to the mechanism of crystallization of perovskites in a purely KOH environment, only cubic crystals can be prepared under these conditions; by introduction of NH_4^+, various final crystal shapes emerge.

2.1 Sample preparation

Sample preparation was adapted from previously reported methods.[25,28] In detail, solutions of $La(NO_3)_3$, $Sr(NO_3)_2$, and $KMnO_4$ were injected into a beaker with continuous magnetic stirring. Then some amount of water was added to modulate the concentration of solution. KOH was poured into the beaker and dissolved gradually in the solution to work as a mineralizer. After the solution was cooled down to room temperature, $MnCl_2$ was added to modulate the valancey balance in the final compounds. Finally, urea was poured into the mixture of solutions in the beaker. The specific amounts of each of the starting chemicals are listed in Table 1. The whole mixture was transferred into a 60 mL Teflon autoclave with a filling capacity of *ca.* 75% and then kept at 240 °C for 48 h for the $La_{0.75}Sr_{0.25}MnO_3$ sample and 16 h at 260 °C followed by 16 h cooling to room temperature for the $La_{0.5}Sr_{0.5}MnO_3$ sample. After reaction, the final black magnetic samples were washed with deionized water several times and dried at 70 °C for 2 h.

2.2 Characterization

Product composition was determined by inductively coupled plasma spectroscopy (ICP) and confirmed quite well by energy dispersive spectroscopy (EDS). Powder X-ray diffraction (XRD) data were collected on a Rigaku D/Max 2500 V/PC X-ray diffractometer with CuKα radiation (λ = 1.5418 Å) at 50 kV and 200 mA with a scan speed of 1° min^{-1} at room temperature. The step scanning was in the angle range of $10° \leq 2\theta \leq 70°$ with an increment of 0.02°. Scanning electron microscope (SEM) images were recorded with a Helios NanoLab 600i Dual Beam System, FEI Company, America.

3. Results and discussion

3.1 Crystal structure discussion

The crystal phase in $La_{1-x}Sr_xMnO_3$ is strongly related to the ratio of La/Sr at the A-site (Fig. 1). When the ratio of La/Sr = 3, the crystal can be indexed into a slightly tilted (a = 5.471 Å, b = 7.768 Å, c = 5.529 Å; $\alpha = \beta = 90°$, $\gamma = 90.52°$) monoclinic phase (space group: $P2_1/a$), and all peaks are in agreement with previous reports (JCPDS card no. 49-0595).[30] This structure of $La_{1-x}Sr_xMnO_3$ is closely related to orthogonal phases with slightly tilted γ angles in the primitive cell, with $a_p = a/\sqrt{2}$ = 3.869 Å, $b_p = b/2$ = 3.884 Å, $c_p = c/\sqrt{2}$ = 3.910 Å.

$La_{0.5}Sr_{0.5}MnO_3$, the crystal grown by the hydrothermal method, however, was indexed to a pseudo-cubic space group with a = 3.849 Å. Thus, the same effect induced by NH_4^+ occurs on each side of this crystal in contrast to the asymmetrical effect on $La_{0.75}Sr_{0.25}MnO_3$ crystals. As indicated in our previous report, in the orthorhombic phase, the exposed crystal facet is the {110} facet. This phenomenon was confirmed in this paper as seen in the XRD and following SEM data (Fig. 2 and 3).

Table 1 Amount of each starting chemicals for preparation of LSMO samples[a]

Sample name	$La(NO_3)_3$ (mL)	$Sr(NO_3)_2$ (mL)	$KMnO_4$ (mL)	H_2O (mL)	KOH (g)	$MnCl_2$ (mL)	Urea (g)
$La_{0.75}Sr_{0.25}MnO_3$	6.25	2.09	2.31	15.11	18	4.46	4.83
$La_{0.5}Sr_{0.5}MnO_3$	5.83	5.83	3.00	20.76	20	6.10	5.61

[a] The addition order of starting chemicals was from left to right, *i.e.* from $La(NO_3)_3$ to urea step by step.

3.2 Shape diversity in both samples

As can be seen in Fig. 2 and 3, when the ratio of La/Sr = 1, the interaction of NH_4^+ with the LSMO crystal surface is mainly on the {111} facets, which may be due to the pseudo-cubic crystal structure. For the pseudo-cubic group, $a = b = c$, which means the capping effect toward each axis is equal, and this results in a symmetrical {111} facet evolution process (Fig. 2). When the ratio of La/Sr = 3, LSMO crystallized in a slightly tilted orthogonal structure (Fig. 1), with unequal lattice parameters a, b and c. The effect of NH_4^+ towards crystals of this structure results in a growth process that is outwardly reducing in further {100} facets (Fig. 3).

In traditional hydrothermally-prepared $La_{1-x}Sr_xMnO_3$, with KOH as a mineralizer, only cubic-shaped crystals could be achieved. By introducing NH_4^+ into the reaction mixture for $La_{0.75}Sr_{0.25}MnO_3$, the {100} facets grow coarsely, which may indicate that NH_4^+ has a destructive effect toward the face-shaping process (Fig. 3(a)). In one-pot samples, we can trace the evolution of the crystal shapes. The native crystal outer surface is enclosed with {100} facets in the $La_{0.75}Sr_{0.25}MnO_3$ samples. The presence of NH_4^+ produces active facets and further crystal growth along these active sites occurs. Along the {100} facets, the rough island grows longer and inwardly towards the face centre on each edge (Fig. 3(b)), and finally becomes a pyramid on each side of the {100} facets (Fig. 3(c) and (d)).

In $La_{0.5}Sr_{0.5}MnO_3$ crystals, however, the electrostatic interaction between NH_4^+ and the crystal faces was mainly in the {111} direction. Firstly, the whole {111} facet evolves in the eight corners with a triangular shape (Fig. 2(a)). However, unlike the {100} facet terminated with a smooth La–O layer, the BO_6 octahedra terminated with the {111} surface become rougher due to the poor stability and more active surface energy of these facets. The shapes of the crystals grow from cuboctahedral (Fig. 2(a)) to truncated octahedral (Fig. 2(b)) to eventually octahedral (Fig. 2(c)). However, an inwardly-directed dissolving effect may result in facet corruption along the {111} axis, which gradually changes the shape of the

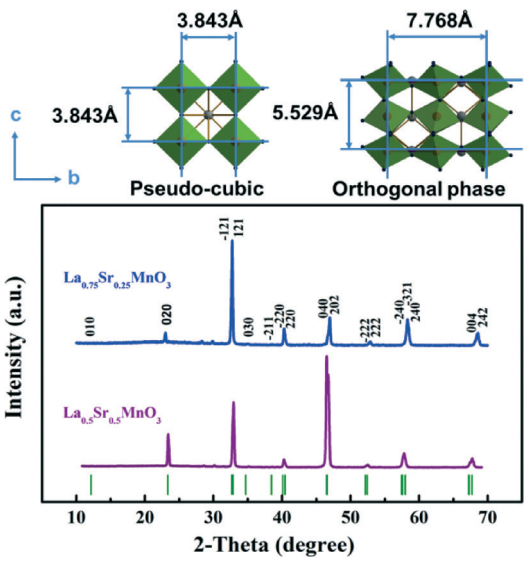

Fig. 1 XRD analysis of as-prepared $La_{0.75}Sr_{0.25}MnO_3$ and $La_{0.5}Sr_{0.5}MnO_3$ samples, the vertical green bars are indicated peak positions of JCPDS card no. 49-0595.

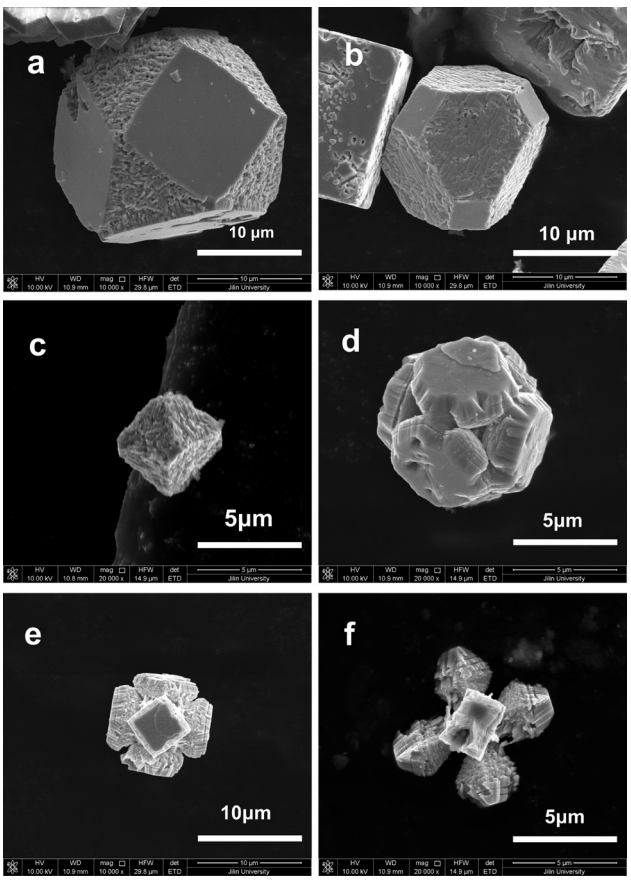

Fig. 2 Shape diversity of $La_{0.5}Sr_{0.5}MnO_3$: (a) cuboctahedral, (b) truncated octahedral, (c) octahedral, (d) inwardly etched cubic along {111} directions, (e) further inward crystal etching with 6 pyramid knots at their tops, (f) final fractal shape of crystal.

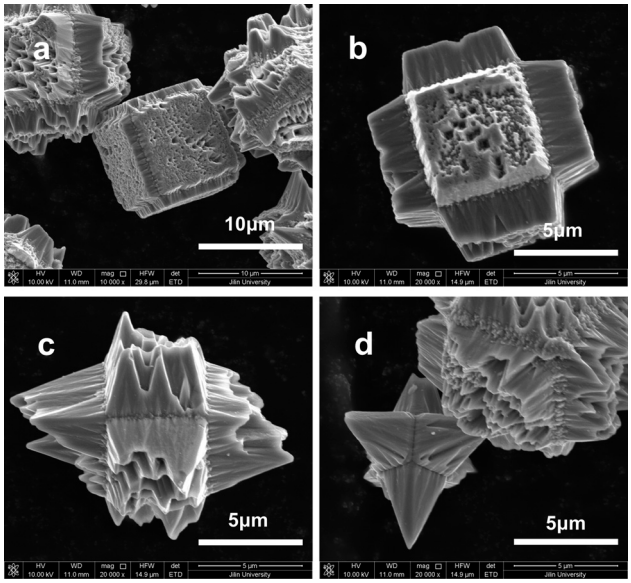

Fig. 3 Shape evolution of $La_{0.75}Sr_{0.25}MnO_3$ crystals grown in a 260 °C hydrothermal environment: (a) crystal with rough assembly of {100} facets enclosed surface, (b) further growth along {100} direction but toward the face centre, (c) and (d) half and fully grown 6 pyramids along {100} axis.

crystals (Fig. 2(d) and (e)) and finally produces a fractal pyramid shape (Fig. 2(f)).

3.3 Temperature effect

Reaction temperature plays an important role in crystal formation and shape change, due to nucleation and further directional ripening and growth in a direction dependent on the ion attachment. At 260 °C, the crystals are uniform in size and cubic in shape, which shows a weak effect, even at higher concentrations of NH_4^+. When lowering the temperature to 240 °C, at a urea content of 4.83 g, the shapes of crystals show more diversity within the same pot. By cooling the autoclaves gradually, the final crystals show interesting inward growth.

4. The formation mechanism of various shapes of $La_{1-x}Sr_xMnO_3$ crystals

NH_4^+ plays an important role in the preparation of various shapes of $La_{1-x}Sr_xMnO_3$ crystals, which is confirmed in various crystal samples in previous reports.[18] We propose an electrostatic interaction between the MnO_6 octahedron (the building block of the crystal) and NH_4^+ during the crystallization process. The negatively-charged MnO_6 octahedron is inclined to attract positive cations in the reactive system. According to the chemical balance of the solutions, the cations are K^+, La^{3+} (Sr^{2+}) and NH_4^+ in the reaction environment (Mn is coordinated by O^{2-} or OH^-, which forms the negatively charged MnO_6 cluster *via* d^2sp^3 orbital hybridization between Mn and O).[32] La^{3+} (Sr^{2+}) ions are enclosed by eight MnO_6 octahedra to balance the negative charge, forming the final perovskite-structured crystals. K^+ is weakly attached to the surfaces of the MnO_6 octahedra during the propagation of the perovskite unit cell, and is substituted by La^{3+} (Sr^{2+}) after the growth of a further unit on the surface. NH_4^+, however, which is a cation with a non-spherical electric field, may attach to the MnO_6 unit, forming the linkage N–H···O–Mn (Scheme 1). The possible hydrogen bond makes the attachment of NH_4^+ directional, which may block the attachment of La^{3+} (Sr^{2+}) in this position and reduce further propagation of neighbouring MnO_6 octahedra. By this route, the crystal growth in the {111} direction is slowed down, forming the final triangle shapes on the vertices of the previously cubic structure (Fig. 4).

For $La_{0.75}Sr_{0.25}MnO_3$ and $La_{0.5}Sr_{0.5}MnO_3$ samples, these crystallized in different space groups with different cell parameters. The effect of NH_4^+ toward each side of the unit cell is equal in $La_{0.5}Sr_{0.5}MnO_3$ because of the equal lengths of *a*, *b* and *c*. The structural discrepancy yields the evolution of different final shapes. The probability of the attachment of NH_4^+ is equal for the eight faces of the octahedron, theoretically. Thus, it is still a challenge to control crystal growth along uniform facets in the samples.

This work is generally applicable to other cations with non-spherical electric fields in the modulation of crystal facets, and the facet-dependent properties may potentially lead to practical applications.

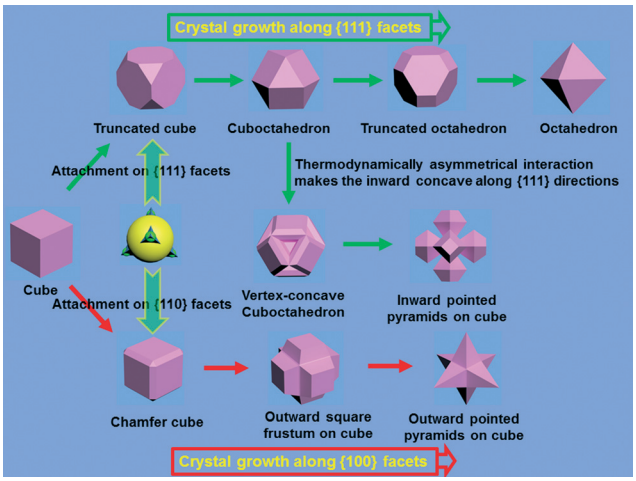

Fig. 4 Schematic of $La_{1-x}Sr_xMnO_3$ crystal shape evolution in NH_4^+ environment: for La/Sr = 1 crystals, the effect of NH_4^+ is to limit the growing speed of the {111} facets to some degree, from truncated cubes to cuboctahedra and finally octahedra; however, the interactive region is not always uniform on the MnO_6 octahedral faces, the capping effect may work along the {111} direction, which makes the vertex-concave cuboctahedron and finally pyramids pointed inwardly towards the central cube; for La/Sr = 3 crystals, these crystallize in a nearly orthogonal phase, and the interaction of NH_4^+ with the MnO_6 octahedra causes further growth along the {100} facets, with inwardly-directed growth, which finally forms outward-pointed pyramids on the inner cubes.

5. Conclusion

In summary, shape diversity of $La_{1-x}Sr_xMnO_3$ crystals was acquired from a mild hydrothermal environment in which NH_4^+ plays a role as a facet growth modulator. By adjusting the La/Sr ratio at the A-sites of this perovskite manganite, the structures of the final crystals evolved, due to different facet evolution processes. An NH_4^+ accommodation mechanism was proposed to explain the shape diversity in one pot. This idea builds a fundamental understanding of crystal facet modulation by introducing cations with non-spherical symmetry to the reactive environment.

Acknowledgements

This work was supported by the National Natural Science Foundation of China (grants 90922034, 21131002, and 21201075) and the Specialized Research Fund for the Doctoral Program of Higher Education (SRFDP grant 20110061130005), and the Natural Science Foundation of Jilin Province (grants 20140520080JH).

Notes and references

1 Y.-W. Jun, J.-S. Choi and J. Cheon, *Angew. Chem., Int. Ed.*, 2006, **45**, 3414–3439.
2 Y. Bi, S. Ouyang, N. Umezawa, J. Cao and J. Ye, *J. Am. Chem. Soc.*, 2011, **133**, 6490–6492.
3 B. Geng, C. Fang, F. Zhan and N. Yu, *Small*, 2008, **4**(9), 1337–1443.
4 J. Ren, W. Wang, S. Sun, L. Zhang, L. Wang and J. Chang, *Ind. Eng. Chem. Res.*, 2011, **50**, 10366–10369.
5 R. Long, K. Mao, X. Ye, W. Yan, Y. Huang, J. Wang, F. Yao, X. Wang, X. Wu, Y. Xie and Y. Xiong, *J. Am. Chem. Soc.*, 2013, **135**, 3200–3207.
6 B. Lim, M. Jiang, J. Tao, P. H. C. Camargo, Y. Zhu and Y. Xia, *Adv. Funct. Mater.*, 2009, **19**, 189–200.
7 J. Chen, B. Lim, E. P. Lee and Y. Xia, *Nano Today*, 2009, **4**, 81–95.
8 A. R. Tao, S. Habas and P. Yang, *Small*, 2008, **4**(3), 310–325.
9 M. Leng, M. Liu, Y. Zhang, Z. Wang, C. Yu, X. Yang, H. Zhang and C. Wang, *J. Am. Chem. Soc.*, 2010, **132**, 17084–17087.
10 (*a*) M. M. Maitani, K. Tanaka, D. Mochizuki and Y. Wada, *J. Phys. Chem. Lett.*, 2011, **2**, 2655–2659; (*b*) Y. Luan, L. Jing, Y. Xie, X. Sun, Y. Feng and H. Fu, *ACS Catal.*, 2013, **3**, 1378–1385; (*c*) G. Liu, H. G. Yang, J. Pan, Y. Q. Yang, G. Q. (Max) Lu and H.-M. Cheng, *Chem. Rev.*, 2014, DOI: 10.1021/cr400621z.
11 (*a*) X. Xie, Y. Li, Z.-Q. Liu, M. Haruta and W. Shen, *Nature*, 2009, **458**, 746–749; (*b*) L. Hu, Q. Peng and Y. Li, *J. Am. Chem. Soc.*, 2008, **130**, 16136–16137.
12 B. Shao, Q. Zhao, N. Guo, Y. Jia, W. Lv, M. Jiao, W. Lü and H. You, *Cryst. Growth Des.*, 2013, **13**, 3582–3587.
13 C. Hou, W. Feng, L. Yuan, K. Huang and S. Feng, *CrystEngComm*, 2014, **16**, 2874–2877.
14 (*a*) H. Wen, M. Cao, G. Sun, W. Xu, D. Wang, X. Zhang and C. Hu, *J. Phys. Chem. C*, 2008, **112**, 15948–15955; (*b*) Z. Li, X. Lai, H. Wang, D. Mao, C. Xing and D. Wang, *Nanotechnology*, 2009, **20**, 245603; (*c*) Z. Li, X. Lai, H. Wang, D. Mao, C. Xing and D. Wang, *J. Phys. Chem. C*, 2009, **113**, 2792–2797.
15 (*a*) C. Bullen, P. Zijlstra, E. Bakker, M. Gu and C. Raston, *Cryst. Growth Des.*, 2011, **11**, 3375–3380; (*b*) T. Ming, W. Feng, Q. Tang, F. Wang, L. Sun, J. Wang and C. Yan, *J. Am. Chem. Soc.*, 2009, **131**, 16350–16351.
16 L. Fan and R. Guo, *Cryst. Growth Des.*, 2008, **8**, 2150–2156.
17 L. Fei, J. Yuan, Y. Hu, C. Wu, J. Wang and Y. Wang, *Cryst. Growth Des.*, 2011, **11**, 1049–1053.
18 H. Zhan, X. Yang, C. Wang, J. Chen, Y. Wen, C. Liang, H. F. Greer, M. Wu and W. Zhou, *Cryst. Growth Des.*, 2012, **12**, 1247–1253.
19 T. Toshima, H. Ishikawa, S. Tanda and T. Akiyama, *Cryst. Growth Des.*, 2008, **8**(7), 2066–2069.
20 H. Kato, M. Kobayashi, M. Hara and M. Kakihana, *Catal. Sci. Technol.*, 2013, **3**, 1733–1738.
21 (*a*) J. Zhu, S. Wang, S. Xie and H. Li, *Chem. Commun.*, 2011, **47**, 4403–4405; (*b*) Z.-G. Zhao, Z.-F. Liu and M. Miyauchi, *Chem. Commun.*, 2010, **46**, 3321–3323.
22 V. Kumar, X. Wang and P. S. Lee, *CrystEngComm*, 2013, **15**, 7663–7669.
23 X. Han, X. Wang, S. Xie, Q. Kuang, J. Ouyang, Z. Xie and L. Zheng, *RSC Adv.*, 2012, **2**, 3251–3253.
24 D. Wang, R. Yu, S. Feng, W. Zheng, T. Takei, N. Kumada and N. Kinomura, *Solid State Ionics*, 2002, **151**, 329–333.
25 M. A. Peña and J. L. G. Fierro, *Chem. Rev.*, 2001, **101**, 1981–2017.
26 S. Royer and D. Duprez, *ChemCatChem*, 2011, **3**, 24–65.
27 S. Liang, F. Teng, G. Bulgan and Y. Zhu, *J. Phys. Chem. C*, 2007, **111**, 16742–16749.
28 C. H. Kim, G. Qi, K. Dahlberg and W. Li, *Science*, 2010, **327**, 1624–1627.
29 K. A. Stoerzinger, M. Risch, J. Suntivich, W. M. Lü, J. Zhou, M. D. Biegalski, H. M. Christen, Ariando, T. Venkatesan and S.-H. Yang, *Energy Environ. Sci.*, 2013, **6**, 1582–1588.
30 X. Chu, K. Huang, M. Han and S. Feng, *Inorg. Chem.*, 2013, **52**(8), 4130–4132.
31 K. Huang, X. Chu, W. Feng, C. Zhou, W. Si, X. Wu, L. Yuan and S. Feng, *Chem. Eng. J.*, 2014, **244**, 27–32.
32 G. Zheng and C. H. Patterson, *Phys. Rev. B: Condens. Matter Mater. Phys.*, 2003, **67**, 220404.

